INTERNATIONAL JOURNAL FOR NUMERICAL METHODS IN FLUIDS
Int. J. Numer. Meth. Fluids 2001; **35**: 421–447

Control of vortex shedding behind circular cylinder for flows at low Reynolds numbers

S. Mittal*,[1] and A. Raghuvanshi

Department of Aerospace Engineering, Indian Institute of Technology, Kanpur, India

SUMMARY

It has been observed by researchers in the past that vortex shedding behind circular cylinders can be altered, and in some cases suppressed, over a limited range of Reynolds numbers by proper placement of a second, much smaller, 'control' cylinder in the near wake of the main cylinder. Results are presented for numerical computations of some such situations. A stabilized finite element method is employed to solve the incompressible Navier–Stokes equations in the primitive variables formulation. At low Reynolds numbers, for certain relative positions of the main and control cylinder, the vortex shedding from the main cylinder is completely suppressed. Excellent agreement is observed between the present computations and experimental findings of other researchers. In an effort to explain the mechanism of control of vortex shedding, the streamwise variation of the pressure coefficient close to the shear layer of the main cylinder is compared for various cases, with and without the control cylinder. In the cases where the vortex shedding is suppressed, it is observed that the control cylinder provides a local favorable pressure gradient in the wake region, thereby stabilizing the shear layer locally. Copyright © 2001 John Wiley & Sons, Ltd.

KEY WORDS: finite element; flow control; two cylinders; unsteady flows; vortex shedding control cylinder

1. INTRODUCTION

A large number of engineering structures involve bluff bodies that experience unsteady wind loads which may, in some cases, have a significant influence on their design. Control of vortex shedding leads to a reduction in the unsteady forces acting on the bluff bodies and can significantly reduce their vibrations. Flow control may be accomplished by controlling the boundary layer separation and/or the structure of shear layer(s) in the wake and various methods like blowing, suction, surface roughness elements, etc., have been studied by researchers in the past. Review articles by Gad-el-Hak and Bushnel [1], Griffin and Hall [2], and

* Correspondence to: Department of Aerospace Engineering, Indian Institute of Technology, Kanpur, UP 208 016, India.
[1] E-mail: smittal@iitk.ac.in

Received 17 December 1997
Revised 20 December 1998

Zdravkovich [3] present a fairly comprehensive overview of the various means for suppressing vortex shedding. Zdravkovich [3] presents control techniques that can be classified into three categories: surface protrusions, shrouds, and near-wake stabilizers. He also investigated the relative effectiveness of the various means of flow control by applying them to the same test model, including the multi-cylinder arrangement. Griffin and Hall [2] summarize the possible modification of the wake of a cylinder by its oscillatory motion. More details on the effect of the translational oscillations can be found in the work by Williamson and Roshko [4], Ongoren and Rockwell [5,6], Lecointe *et al.* [7], and Mittal and Tezduyar [8]. Tokumaru and Dimotakis [9,10] have demonstrated via laboratory experiments that a significant control on the structure of the wake can be achieved by subjecting the cylinder to rotary oscillations. Gad-el-Hak and Bushnel [1] review various techniques that are employed for separation control, including the moving-surface boundary layer control in which rotating cylinder elements are employed to inject momentum into the already existing boundary layer. Modi *et al.* [11–13] have employed this concept to increase the maximum lift on airfoils and to reduce the drag on bluff bodies. Preliminary finite element simulations supporting these observations have been presented by Mittal [14].

In an effort to study a passive control device, Strykowski and Sreenivasan [15] have reported that the vortex shedding past a circular cylinder can be controlled over a limited range by the proper placement of a (smaller) control cylinder close to the main cylinder. They have conducted a fairly comprehensive investigation, using laboratory experiments to study the effect of the size and position of the control cylinder on the behavior of the vortex shedding from the main cylinder. They found that there exists a domain close to the main cylinder where the placement of a control cylinder can completely suppress the vortex shedding for flows at a Reynolds number of 80 or less. The actual extent of this domain depends on the Reynolds number of the flow and the ratio of the diameter of the two cylinders. Even though the flow remains unsteady for Reynolds numbers larger than 80, the presence of the control cylinder has a significant effect on the flow. It has also been reported that in certain cases suppression of vortex shedding is accompanied by a significant reduction in the mean drag coefficient.

Kim and Chang [16] have reported their computational results for the same phenomenon using a mixed finite element method–finite difference method (FEM–FDM) technique applied to the vorticity–streamfunction form of the Navier–Stokes equations. Recently, Morzynski *et al.* [17] have applied their eigensolution method for the global non-parallel flow stability analysis to this problem and have computed the critical Reynolds number for instability for certain location of the control cylinder. Their observations are in very good agreement with the experimental results. Flow past two cylinders of equal diameters has been studied extensively by researchers in the past [18–25]. Such flows are quite sensitive to the relative location of the two cylinders and the Reynolds numbers. It has been reported by Mittal *et al.* [25] that for two cylinders arranged in tandem, with a distance of 2.5 diameters between their centers, the flow is steady at Reynolds numbers = 100. However, it becomes unsteady at Reynolds numbers = 1000. Wu and Hu [26] have investigated numerically the flow past two tandem cylinders of unequal diameters for Reynolds number = 200 based on the diameter of the larger, downstream cylinder. They have observed that a reduction in the diameter of the upstream cylinder leads to a decrease in the critical spacing between the two cylinders beyond which vortex shedding takes place behind both cylinders.

In this article, results are presented for numerical computations of some of the cases reported by Strykowski and Sreenivasan [15]. The numerical method that has been employed is same as the one used by Mittal *et al.* [25] to compute flow past two cylinders of equal diameter in staggered and tandem arrangements at Reynolds numbers = 100 and 1000. First, flow past a single cylinder at Reynolds numbers = 60, 70, 80, and 100 is computed and results are compared with those from experiments by other researchers. Next, computations are carried out with a control cylinder, one-seventh the diameter of the main one, located five diameters away, each in the transverse and in-line directions, from the main cylinder. For this arrangement, the effect of the control cylinder on the flow past the main cylinder is expected be negligible. However, the interest here is to study the effect of the unsteady wake of the main cylinder on the control cylinder. In the second set of computations, the control cylinder is placed such that the in-line and cross-flow distances from the main cylinder are two and one cylinder diameters respectively. Strykowski and Sreenivasan [15] have observed that this location of the control cylinder lies marginally outside the region within which the placement of control cylinder results in a complete suppression of the vortex shedding for Reynolds number = 80. The present computations also led to the same observations. The final set of computations correspond to a location of the control cylinder for which Strykowski and Sreenivasan [15] have observed a complete suppression of vortex shedding for Reynolds number = 80. In this arrangement, the in-line location of the control cylinder remains the same as before while the cross-flow distance between the two cylinders is reduced to 0.8 diameters.

In an effort to explain the mechanism of control of vortex shedding, the streamwise variation of the pressure coefficient close to the shear layer of the main cylinder is compared for various cases, with and without the control cylinder. It is observed that in certain cases the control cylinder provides a local favorable pressure gradient in the wake region, thereby stabilizing the shear layer locally. Depending on the magnitude of the favorable pressure gradient, one observes a varied level of unsteadiness/instability of the wake for different cases.

The outline of the rest of the paper is as follows. We begin by reviewing the governing equations for incompressible fluid flow in Section 2. The streamline-upwind/Petrov–Galerkin (SUPG) and pressure-stabilizing/Petrov–Galerkin (PSPG) stabilization techniques [27–29] are employed to stabilize our computations against spurious numerical oscillations and to enable us to use equal-order interpolation velocity–pressure elements. Section 3 describes the finite element formulation incorporating these stabilizing terms. In Section 4 computational results for flows involving a single cylinder and control cylinder are presented and discussed. In Section 5 the results are summarized and a few concluding remarks are made.

2. THE GOVERNING EQUATIONS

Let $\Omega \subset \mathbb{R}^{n_{sd}}$ and $(0, T)$ be the spatial and temporal domains respectively, where n_{sd} is the number of space dimensions, and let Γ denote the boundary of Ω. The spatial and temporal co-ordinates are denoted by $\mathbf{x}$ and t. The Navier–Stokes equations governing incompressible fluid flow are

$$\rho\left(\frac{\partial \mathbf{u}}{\partial t}+\mathbf{u}\cdot\nabla\mathbf{u}-\mathbf{f}\right)-\nabla\cdot\boldsymbol{\sigma}=0 \quad \text{on } \Omega \text{ for } (0, T) \tag{1}$$

$$\nabla\cdot\mathbf{u}=0 \quad \text{on } \Omega \text{ for } (0, T) \tag{2}$$

Here ρ, $\mathbf{u}$, $\mathbf{f}$, and $\boldsymbol{\sigma}$ are the density, velocity, body force, and the stress tensor respectively. The stress tensor is written as the sum of its isotropic and deviatoric parts

$$\boldsymbol{\sigma}=-p\mathbf{I}+\mathbf{T}, \quad \mathbf{T}=2\mu\boldsymbol{\varepsilon}(\mathbf{u}), \quad \boldsymbol{\varepsilon}(\mathbf{u})=\frac{1}{2}((\nabla\mathbf{u})+(\nabla\mathbf{u})^T) \tag{3}$$

where p and μ are the pressure and viscosity respectively. Both the Dirichlet and Neumann-type boundary conditions are accounted for, represented as

$$\mathbf{u}=g \quad \text{on } \Gamma_g, \qquad \mathbf{n}\cdot\boldsymbol{\sigma}=\mathbf{h} \quad \text{on } \Gamma_h \tag{4}$$

where Γ_g and Γ_h are complementary subsets of the boundary Γ. The initial condition on the velocity is specified on Ω

$$\mathbf{u}(\mathbf{x}, 0)=\mathbf{u}_0 \quad \text{on } \Omega \tag{5}$$

where $\mathbf{u}_0$ is divergence free.

3. FINITE ELEMENT FORMULATION

Consider a finite element discretization of Ω into sub-domains Ω^e, $e=1, 2, \ldots, n_{\text{el}}$, where n_{el} is the number of elements. Based on this discretization, for velocity and pressure we define the finite element trial function spaces $\mathscr{S}^h_{\mathbf{u}}$ and $\mathscr{S}^h_p$, and weighting function spaces $\mathscr{V}^h_{\mathbf{u}}$ and $\mathscr{V}^h_p$. These function spaces are selected by taking the Dirichlet boundary conditions into account as subsets of $[\mathbf{H}^{1h}(\Omega)]^{n_{\text{sd}}}$ and $\mathbf{H}^{1h}(\Omega)$, where $\mathbf{H}^{1h}(\Omega)$ is the finite-dimensional function space over Ω. The stabilized finite element formulation of Equations (1) and (2) is written as follows: find $\mathbf{u}^h\in\mathscr{S}^h_{\mathbf{u}}$ and $p^h\in\mathscr{S}^h_p$ such that $\forall\mathbf{w}^h\in\mathscr{V}^h_{\mathbf{u}}$, $q^h\in\mathscr{V}^h_p$

$$\begin{aligned}
&\int_\Omega \mathbf{w}^h\cdot\rho\left(\frac{\partial \mathbf{u}^h}{\partial t}+\mathbf{u}^h\cdot\nabla\mathbf{u}^h-\mathbf{f}\right)\mathrm{d}\Omega+\int_\Omega \boldsymbol{\varepsilon}(\mathbf{w}^h):\ \boldsymbol{\sigma}(p^h, \mathbf{u}^h)\,\mathrm{d}\Omega+\int_\Omega q^h\nabla\cdot\mathbf{u}^h\,\mathrm{d}\Omega\\
&+\sum_{e=1}^{n_{\text{el}}}\int_{\Omega^e}\frac{1}{\rho}(\tau_{\text{SUPG}}\rho\mathbf{u}^h\cdot\nabla\mathbf{w}^h+\tau_{\text{PSPG}}\nabla q^h)\cdot\left[\rho\left(\frac{\partial \mathbf{u}^h}{\partial t}+\mathbf{u}^h\cdot\nabla\mathbf{u}^h-\mathbf{f}\right)-\nabla\cdot\boldsymbol{\sigma}(p^h, \mathbf{u}^h)\right]\mathrm{d}\Omega^e\\
&+\sum_{e=1}^{n_{\text{el}}}\int_{\Omega^e}\delta\nabla\cdot\mathbf{w}^h\rho\nabla\cdot\mathbf{u}^h\,\mathrm{d}\Omega^e=\int_{\Gamma_h}\mathbf{w}^h\cdot\mathbf{h}^h\,\mathrm{d}\Gamma
\end{aligned} \tag{6}$$

In the variational formulation given by Equation (6), the first three terms and the right-hand side constitute the Galerkin formulation of the problem. The first series of element-level

integrals are the SUPG and PSPG stabilization terms added to the variational formulations [27,30]. In the current formulation, τ_{PSPG} is the same as τ_{SUPG} and is given as

$$\tau = \left(\left(\frac{2\|\mathbf{u}^h\|}{h} \right)^2 + \left(\frac{4\nu}{h^2} \right)^2 \right)^{-1/2} \tag{7}$$

The second series of element-level integrals are added to the formulation for numerical stability at high Reynolds numbers. This is a least-squares term based on the continuity equation. The coefficient δ is defined as

$$\delta = \frac{h}{2} \|\mathbf{u}^h\| z \tag{8}$$

where

$$z = \begin{cases} \left(\dfrac{Re_u}{3} \right) & Re_u \leq 3 \\ 1 & Re_u > 3 \end{cases} \tag{9}$$

and Re_u is the cell Reynolds number. Both stabilization terms are weighted residuals and therefore maintain the consistency of the formulation.

4. NUMERICAL SIMULATIONS

All computations reported in this article are carried out on the *Digital* workstations at *IIT Kanpur*. Equal-in-order bilinear basis functions for velocity and pressure and used and a 2×2 Gaussian quadrature is employed for numerical integration. The non-linear equation systems resulting from the finite element discretization of the flow equations are solved using the Generalized Minimal RESidual (GMRES) technique [31] in conjunction with diagonal preconditioners. The diameter of the main cylinder is D_1 while that of the control cylinder is D_2. All results presented in this article involving the control cylinder are with $D_1/D_2 = 7$. Experimental results for this case have been reported by Strykowski and Sreenivasan [15]. In the present calculation, the two cylinders reside in a rectangular domain whose upstream and downstream boundaries are located at five and 15 cylinder diameters respectively from the center of the main cylinder. The upper and lower boundaries are placed at five diameters, each from the center of the main cylinder. The no-slip condition is specified for the velocity on the cylinder wall and free stream values are assigned or the velocity at the upstream boundary. At the downstream boundary we specify a Neumann-type boundary condition for the velocity, which corresponds to zero viscous stress vector. On the upper and lower boundaries, the component of velocity normal to and the component of stress vector along these boundaries is prescribed a zero value. The Reynolds number is based on the diameter of the main cylinder (D_1), free stream velocity, and the viscosity of the fluid. Computations are carried out for various relative

locations of the two cylinders. The non-dimensional distance between the centers of the two cylinders is denoted by P/D_1 in the flow direction and by T/D_1 in the cross-flow direction, as shown in Figure 1. All values for the lift and drag coefficients and the Strouhal number reported in this article have been non-dimensionalized with respect to the diameter of the main cylinder (D_1). In the presentation of results, quantities with subscript '1' refer to the main cylinder while ones with '2' correspond to the control cylinder. All the values for the Strouhal number correspond to the variation of the lift coefficient.

Strykowski and Sreenivasan [15] have conducted laboratory experiments to study the effect of the size and location of the control cylinder on the behavior of the vortex shedding from the main cylinder. As a result of their comprehensive study they have been able to determine, for various values of D_1/D_2, the regions where the placement of a control cylinder can completely suppress the vortex shedding for flows at Reynolds number = 80. In this paper, results are reported for three locations of the control cylinder for various Reynolds numbers. To clearly show the effect of the control cylinder, results are compared with those for flow past a single cylinder at corresponding Reynolds numbers. The first computation involving the main and control cylinders corresponds to $P/D = 5$ and $T/D = 5$. In this arrangement, the effect of the control cylinder on the flow past the main cylinder is expected be negligible. However, the flow past the control cylinder is affected by the unsteady wake of the main cylinder. In the second set of computations, the main and control cylinder locations correspond to $P/D = 2$ and $T/D = 1$, while the final ones are for $P/D = 2$ and $T/D = 0.8$. For the single cylinder cases and for the cases corresponding to $P/D = 5$ and $T/D = 5$, the upstream and lateral boundaries of the computational domain are located at eight diameters each, while the downstream boundary is located at 22.5 diameters from the center of the main cylinder. The finite element mesh employed for the computation of the $P/D = 2$ and $T/D = 0.8$ case is show in Figure 2. This mesh is very typical of the ones used for other cases reported in this article. In all the cases, first the steady state solution is computed for flow past a cylinder at $Re = 100$. This solution is then perturbed by applying, on the main cylinder, a belt-type boundary condition, which consists of a set of counterclockwise and clockwise rotations. Computations are carried out until a periodic solution develops. The unsteady solution at $Re = 100$ is used as an initial condition to compute flows at other Reynolds numbers.

4.1. Flow past a single cylinder

To understand the effect of placing a control cylinder in the flow field it is essential to first study flow past a single cylinder without a control cylinder. Flow past a circular cylinder at

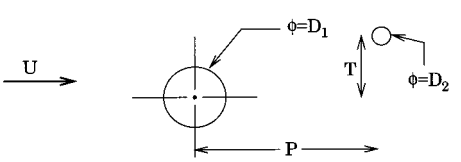

Figure 1. Description of the relative location of the main and control cylinders.

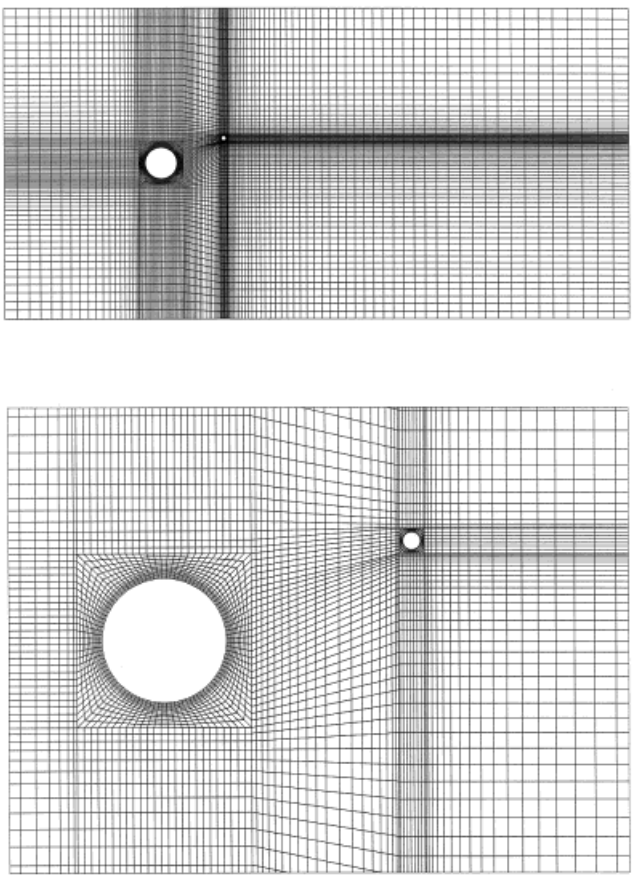

Figure 2. Flow past main and control cylinders, $P/D = 2$, $T/D = 0.8$: finite element mesh (and its close-up) with 10076 nodes and 9816 elements.

$Re = 100$ has become a standard benchmark problem and various researchers in the past have reported their computed results, which are in good agreement with experimental observations [27,30,32,33]. In the paper, results are reported for flow past a single cylinder at $Re = 100$, 80, 70, and 60. The finite element mesh consists of 4209 nodes and 4060 quardrilateral elements. Figure 3 shows the time histories of the lift and drag coefficients for the temporally periodic flows at various Reynolds numbers. For flow at $Re = 100$, the Strouhal number corresponding to the dominant frequency of the lift variations is 0.168, the mean drag coefficient is 1.402, and the amplitude of the lift coefficient is 0.355. These values are in good agreement with those reported elsewhere [27,30,32,33]. From Figure 3 it can be observed that as the Reynolds number is increased, the mean drag coefficient decreases while its time varying component increases. The Strouhal number also increases with the Reynolds number. Table I lists the

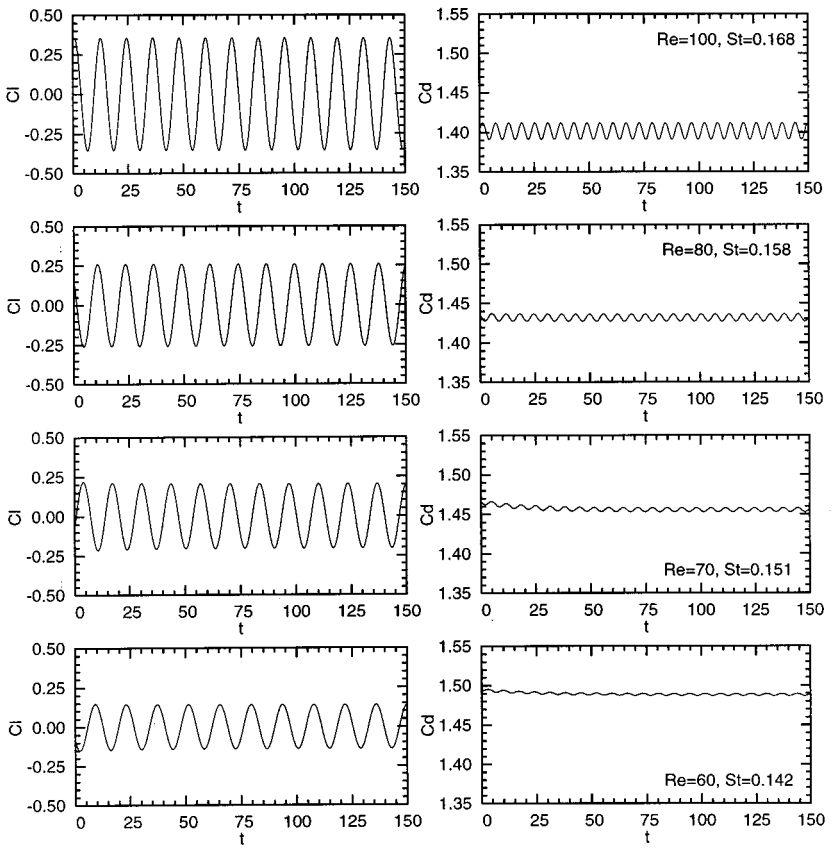

Figure 3. Flow past a single cylinder, $Re = 100$, 80, 70, 60: time histories of the lift and drag coefficients for the temporally periodic solutions.

Table I. Comparison of the computed and experimentally measured values of Strouhal number for flow past a circular cylinder.

Re	*St* (present computations)	*St* (experiments [34] $St = 0.21(1-20/Re)$)
60	0.142	0.140
70	0.151	0.150
80	0.158	0.158
100	0.168	0.168

Strouhal numbers for various Reynolds numbers from the present computations and from measurements from laboratory experiments [34]. The agreement between the two sets of value is quite good.

Figures 4–7 show, respectively for $Re = 100$, 80, 70, and 60, the pressure, streamfunction, and vorticity fields for the temporally periodic solution corresponding to the peak value of the life coefficient. One can observe the well-developed von Karman vortex street in all the solutions and that the unsteadiness in the flow increases with Reynolds number. The same observation can be made by comparing, for different Reynolds numbers, the amplitudes of the lift coefficient and the unsteady component of drag coefficient (see Figure 3).

4.2. $P/D = 5$, $T/D = 5$

When the control cylinder is located far away from the main cylinder, it is expected that the control cylinder has little effect on the main cylinder. Figure 8 shows the pressure, streamfunction, and vorticity fields for the temporally periodic solution corresponding to the peak value of the lift coefficient for the $Re = 100$ flow. Time histories of the drag and lift coefficients for both the main and control cylinders are shown in Figure 9. It can be observed that the flow close to the main cylinder is same as that for a single cylinder, as expected. However, flow in the vicinity of the control cylinder is significantly affected by the unsteady wake of the main cylinder as a result of which the control cylinder experiences unsteady fluid dynamic forces. The Strouhal number corresponding to the variation of lift coefficient for the control cylinder

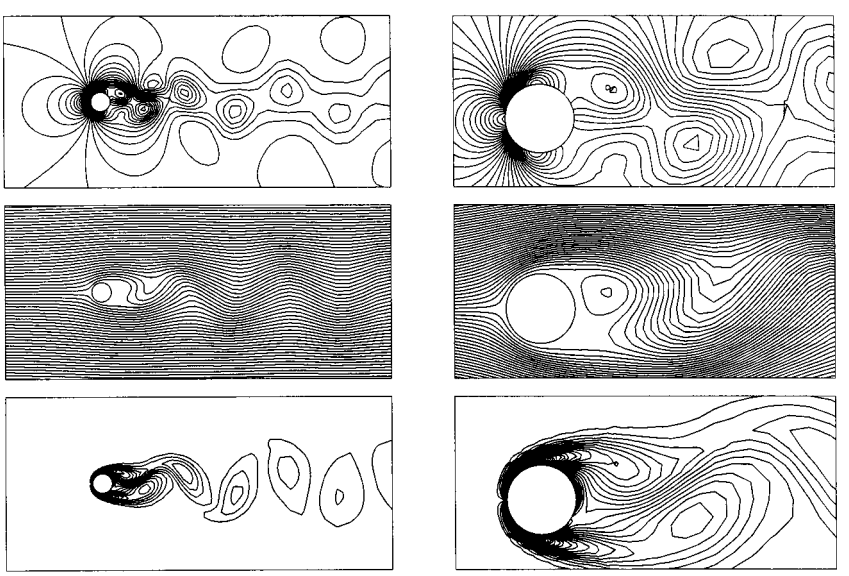

Figure 4. $Re = 100$ flow past a single cylinder: pressure, streamfunction, and vorticity fields for the temporally periodic solution corresponding to the peak value of the lift coefficient.

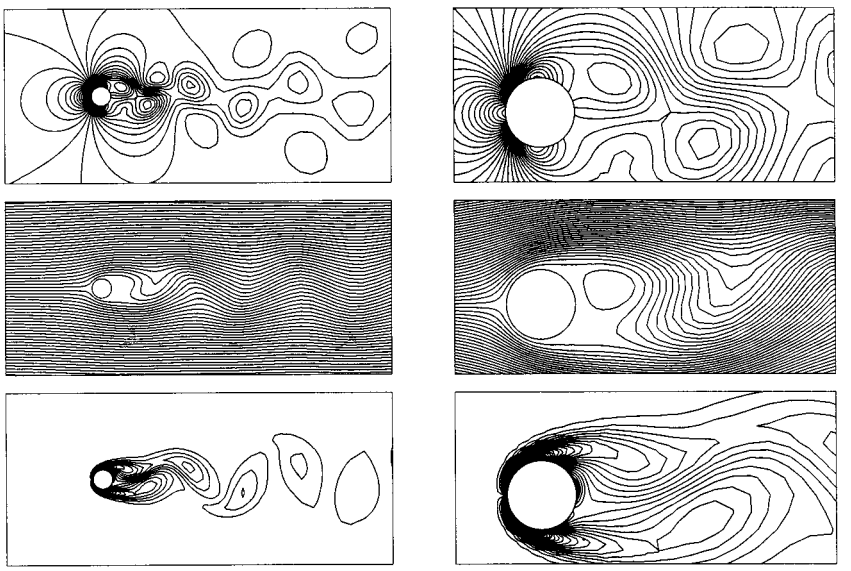

Figure 5. $Re = 80$ flow past a single cylinder: pressure, streamfunction, and vorticity fields for the temporally periodic solution corresponding to the peak value of the lift coefficient.

is the same as that for the main cylinder. However, it must be noticed that there is no vortex shedding past the control cylinder. The Reynolds number based on the free stream speed and the diameter of the control cylinder is 14.3. This is far less than the critical Reynolds number beyond which the shedding takes place for flow past a circular cylinder.

4.3. $P/D = 2$, $T/D = 1$

According to the results reported by Strykowski and Sreenivasan [15], this location of the control cylinder lies marginally outside the region within which the placement of the control cylinder results in a complete suppression of the vortex shedding or $Re = 80$. The computations are first carried out for $Re = 100$ flow. When the fully developed temporally periodic solution is realized, the Reynolds number is changed to 80. Figure 10 shows the pressure, streamfunction, and vorticity fields for the temporally periodic solution corresponding to the peak value of the lift coefficient for the $Re = 100$ flow. Time histories of the drag and lift coefficients for both the main and control cylinders are shown in Figure 11. Compared with the single cylinder case, the Strouhal number for the present case is marginally higher, while the amplitude of the lift coefficient and the mean drag coefficients are lower. From the flow pictures it can be observed that the vortex shedding from the lower surface of the main cylinder, in the presence of control cylinder, is quite similar to that for single cylinder. However, significant interaction takes place between the control cylinder and the vortices formed at the upper surface of the main cylinder. The unsteadiness of the flow on the upper surface of the main cylinder is

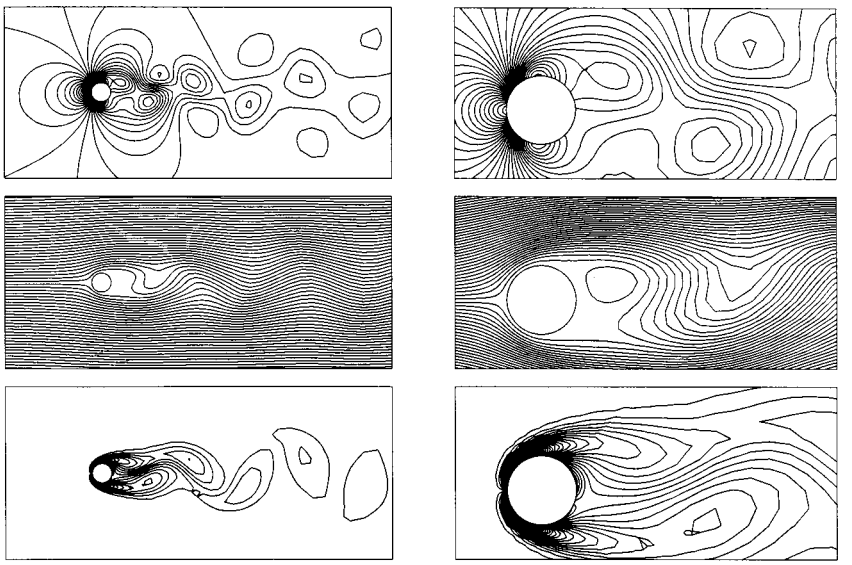

Figure 6. $Re = 70$ flow past a single cylinder: pressure, streamfunction, and vorticity fields for the temporally periodic solution corresponding to the peak value of the lift coefficient.

significantly less than that at the lower surface. Consequently, unlike the single cylinder case, the drag coefficient for the main cylinder in the present case oscillates with the same frequency as the lift coefficient.

When the unsteady flow at $Re = 100$ attains a fully developed state, the Reynolds number is abruptly changed to 80. The solution at $Re = 80$ is shown in Figures 12 and 13. As reported by Strykowski and Sreenivasan [15], the flow at $Re = 80$ is unsteady. Flows for $Re = 70$ and 60 are computed in the same manner by an abrupt decrease in the Reynolds number. The solution corresponding to $Re = 70$ is shown in Figures 14 and 15, while that for $Re = 60$ is shown in Figures 16 and 17. It can be observed that the unsteadiness in the flow decreases as the Reynolds number is reduced and finally at $Re = 60$, the flow reaches a steady state. It should be noticed that the initial condition for the computation at $Re = 60$ is an unsteady solution. Therefore, in that sense the present solution at $Re = 60$ is stable for reasonably large perturbations. Recall the flow past a single cylinder at $Re = 60$ is unsteady for similar levels of perturbations to the initial steady solution (see Figures 3 and 7). Therefore, the stability of the present solution can be attributed to the presence of control cylinder. It is interesting to observe that the $Re = 60$ flow past a cylinder becomes stable in the presence of a 'control' cylinder even though this geometry is inherently asymmetric. At a later stage in this paper, a possible explanation for this stabilization of flow rendered by the control cylinder will be discussed.

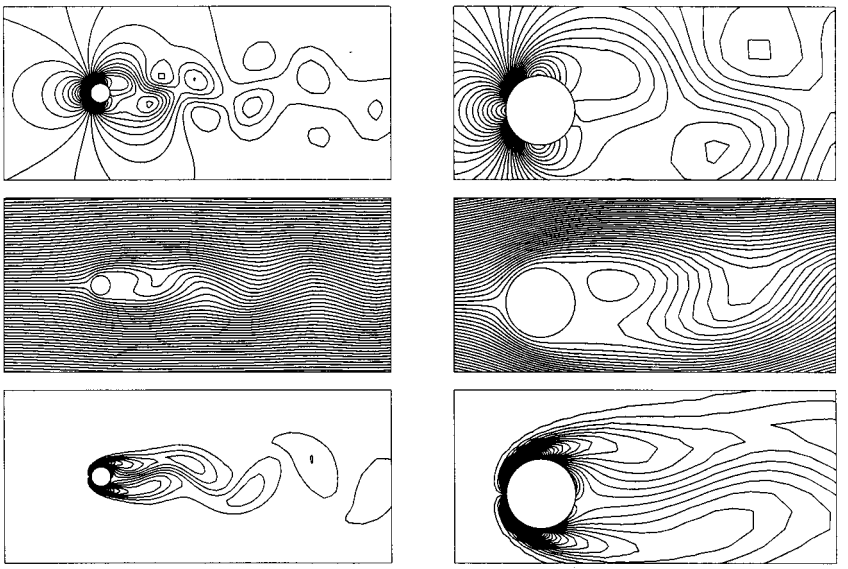

Figure 7. $Re = 60$ flow past a single cylinder: pressure, streamfunction, and vorticity fields for the temporally periodic solution corresponding to the peak value of the lift coefficient.

4.4. $P/D = 2$, $T/D = 0.8$

For this arrangement of the main and control cylinders, Strykowski and Sreenivasan [15] report that the vortex shedding for $Re = 80$ is completely suppressed. Computations are first carried out for $Re = 100$ flow. Figure 18 shows the pressure, streamfunction, and vorticity fields for the temporally periodic solution corresponding to the peak value of the lift coefficient for the $Re = 100$ flow. Time histories of the drag and lift coefficients for both the main and control cylinders are shown in Figure 19. Compared with the single cylinder case and with the case in the previous section for $T/D = 1.0$, the unsteadiness in the flow for the present case is at a lower level, which is indicated by lower values of the Strouhal number, amplitude of the unsteady lift coefficient, and the mean drag coefficient.

The fully developed unsteady flow at $Re = 100$ is used as an initial condition to compute flow at $Re = 80$. In accordance with the observations of Strykowski and Sreenivasan [15], the present computations reveal that the flow at $Re = 80$ attains a steady state. The steady state pressure, streamfunction, and vorticity fields at $Re = 80$ are shown in Figure 20. The time histories of the drag and lift coefficients for the two cylinders are shown in Figure 21. The steady state drag coefficient of the main cylinder is lower than the mean drag coefficient for a single cylinder at $Re = 80$. However, it is accompanied by an additional drag acting on the control cylinder. Therefore, the unsteadiness in the flow past a cylinder at $Re = 80$ can be eliminated completely by placing a control cylinder at the current position but at the expense of increased drag coefficient for the two-cylinder system. Strykowski and Sreenivasan [15] have

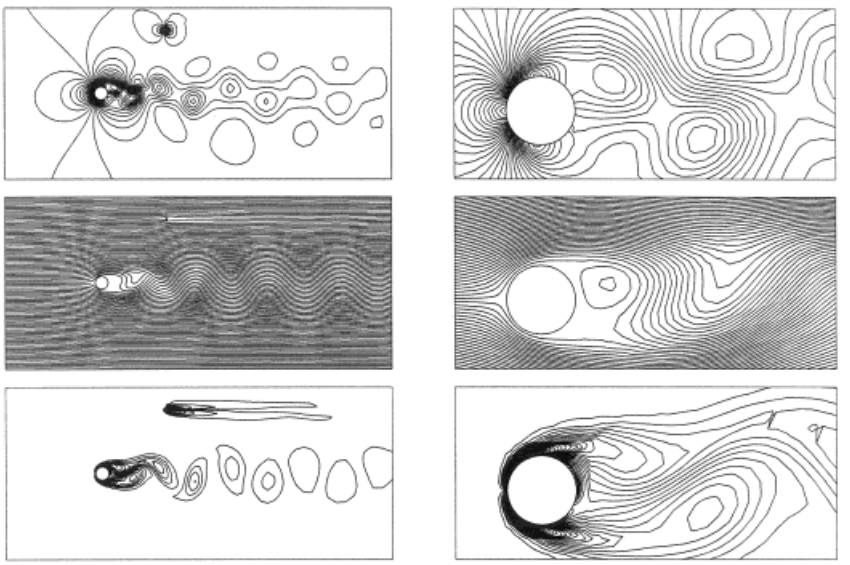

Figure 8. $Re = 100$ flow past main and control cylinders, $P/D = 5$, $T/D = 5$: pressure, streamfunction, and vorticity fields for the temporally periodic solution corresponding to the peak value of the lift coefficient.

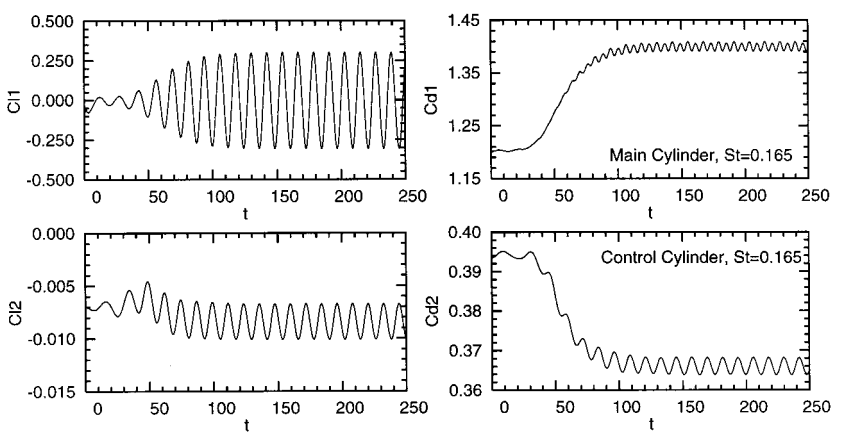

Figure 9. $Re = 100$ flow past main and control cylinders, $P/D = 5$, $T/D = 5$: time histories of the drag and lift coefficients for the main and control cylinders.

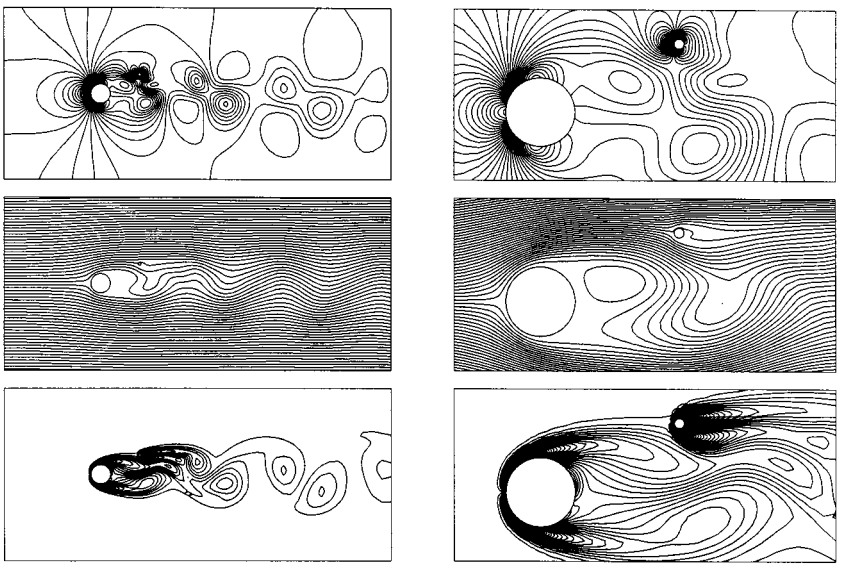

Figure 10. $Re = 100$ flow past main and control cylinders, $P/D = 2$, $T/D = 1$: pressure, streamfunction, and vorticity fields for the temporally periodic solution corresponding to the peak value of the lift coefficient.

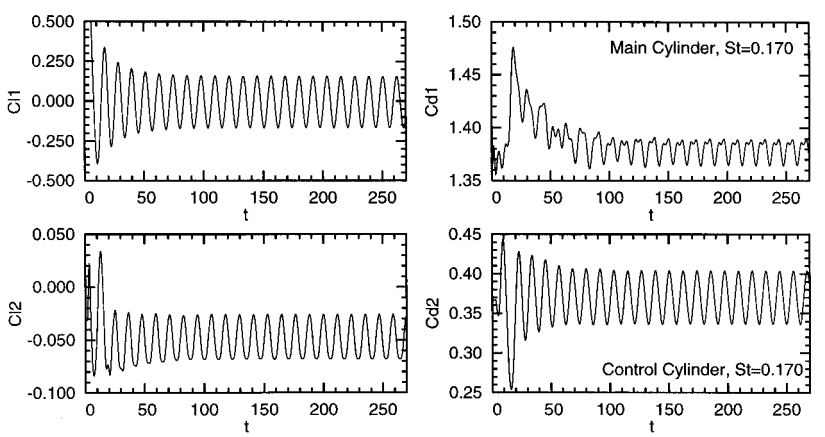

Figure 11. $Re = 100$ flow past main and control cylinders, $P/D = 2$, $T/D = 1$: time histories of the drag and lift coefficients for the main and control cylinders.

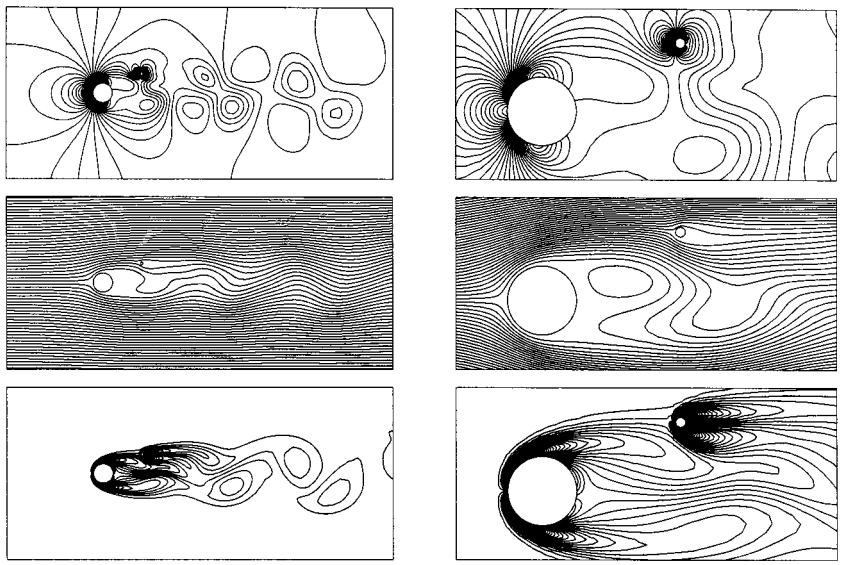

Figure 12. $Re = 80$ flow past main and control cylinders, $P/D = 2$, $T/D = 1$: pressure, streamfunction, and vorticity fields for the temporally periodic solution corresponding to the peak value of the lift coefficient.

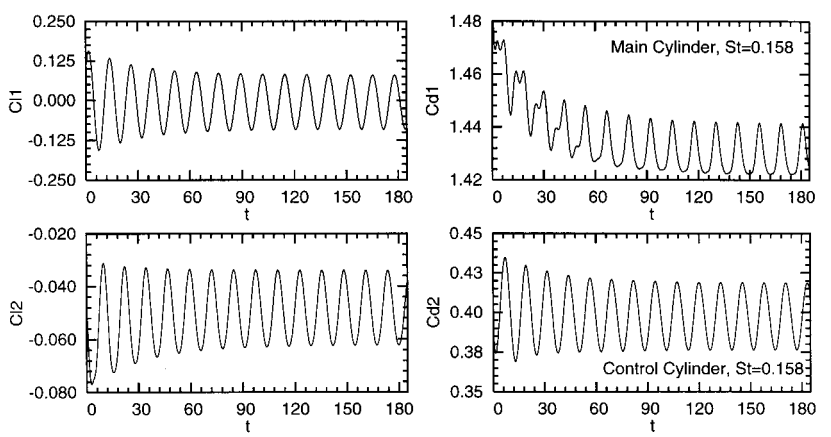

Figure 13. $Re = 80$ flow past main and control cylinders, $P/D = 2$, $T/D = 1$: time histories of the drag and lift coefficients for the main and control cylinders.

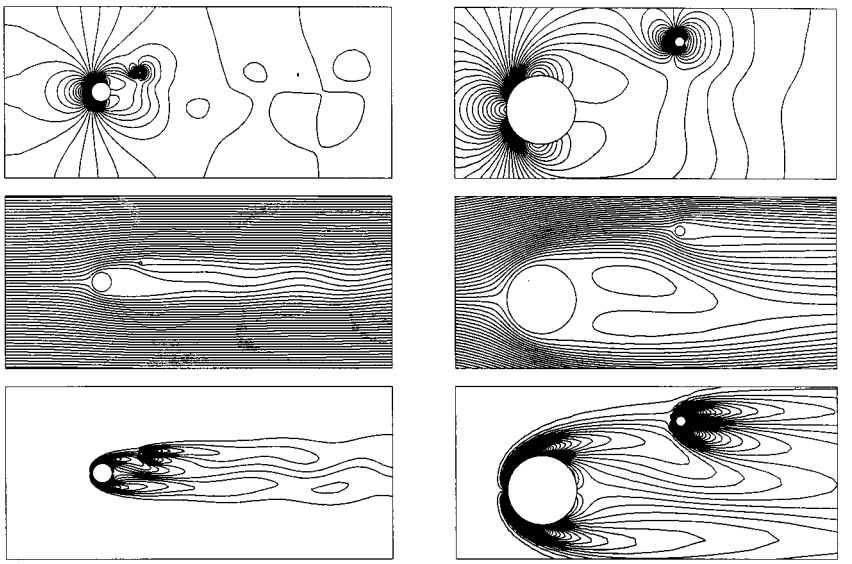

Figure 14. $Re = 70$ flow past main and control cylinders, $P/D = 2$, $T/D = 1$: pressure, streamfunction, and vorticity fields for the temporally periodic solution corresponding to the peak value of the lift coefficient.

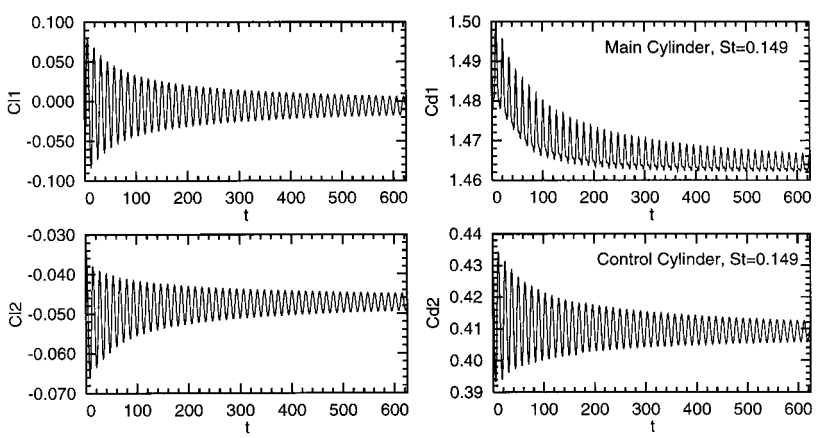

Figure 15. $Re = 70$ flow past main and control cylinders, $P/D = 2$, $T/D = 1$: time histories of the drag and lift coefficients for the main and control cylinders.

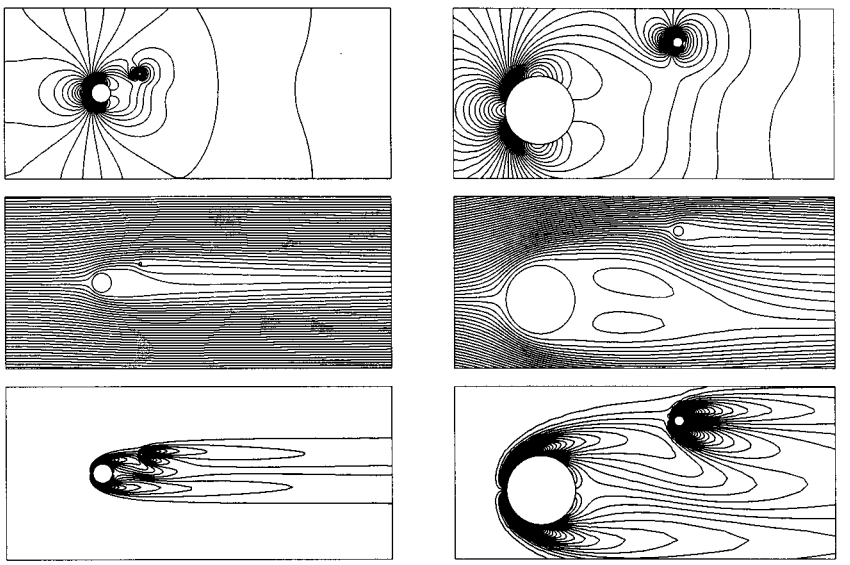

Figure 16. $Re = 60$ flow past main and control cylinders, $P/D = 2$, $T/D = 1$: pressure, streamfunction, and vorticity fields for the steady state solution.

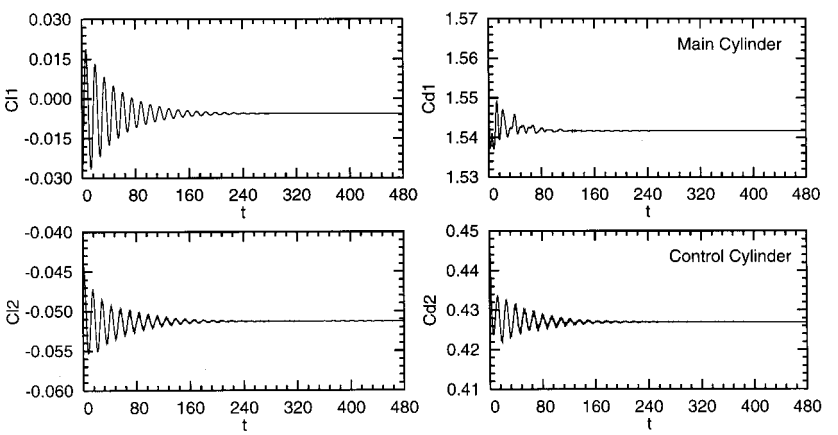

Figure 17. $Re = 60$ flow past main and control cylinders, $P/D = 2$, $T/D = 1$: time histories of the drag and lift coefficients for the main and control cylinders.

observed that it is possible to find an optimal location for the control cylinder such that suppression of vortex shedding at $Re = 80$ leads to about 20 per cent reduction in drag. Figure 22 shows the pressure and vorticity fields at various time instants of this simulation. It can be

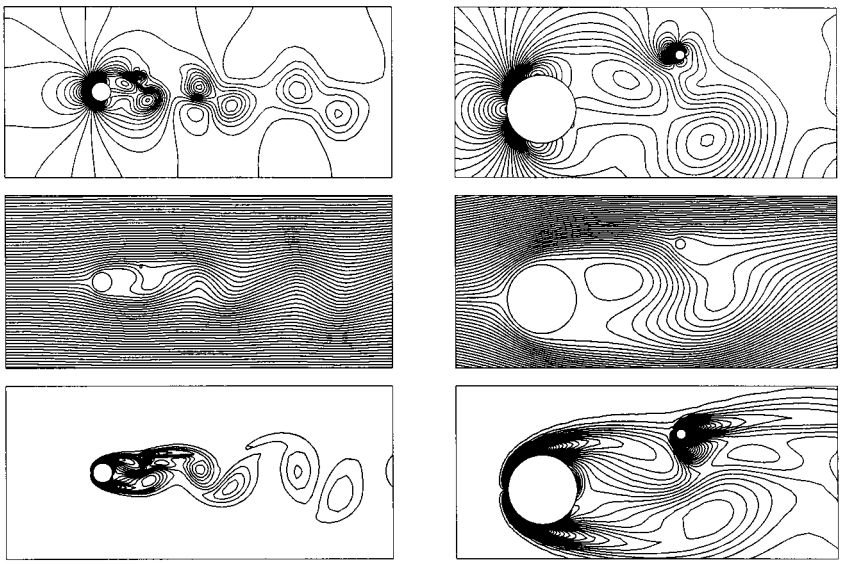

Figure 18. $Re = 100$ flow past main and control cylinders, $P/D = 2$, $T/D = 0.8$: pressure, streamfunction, and vorticity fields for the temporally periodic solution corresponding to the peak value of the lift coefficient.

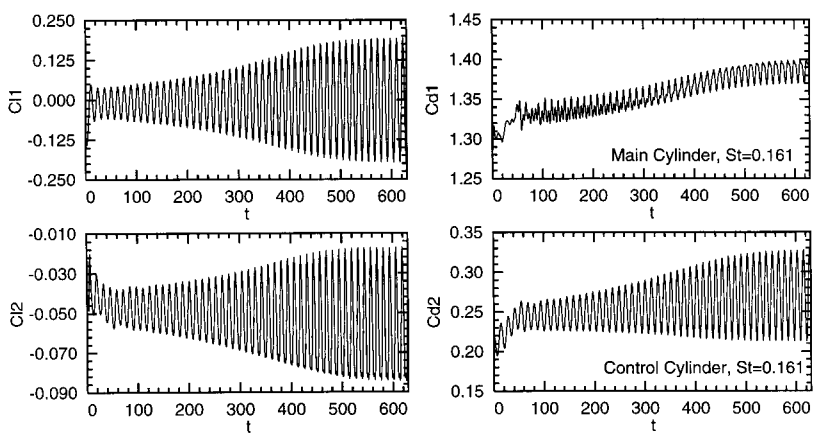

Figure 19. $Re = 100$ flow past main and control cylinders, $P/D = 2$, $T/D = 0.8$: time histories of the drag and lift coefficients for the main and control cylinders.

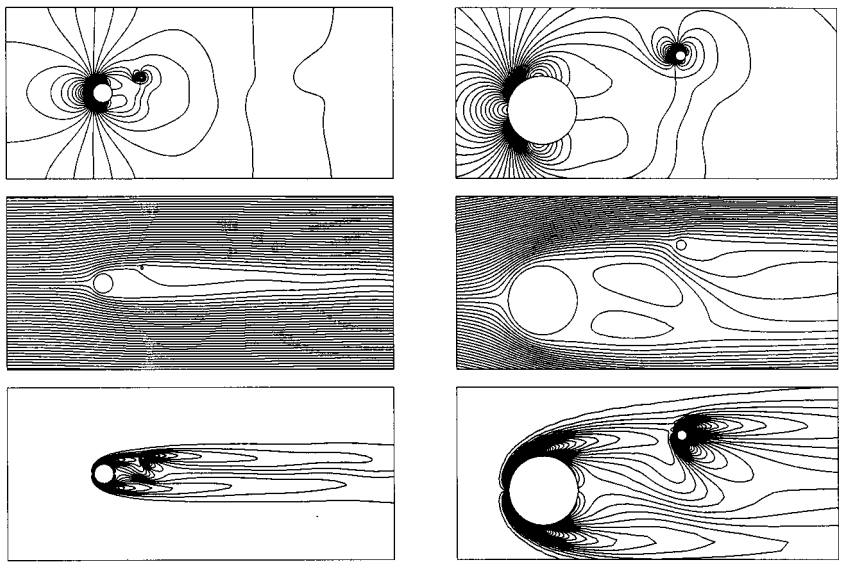

Figure 20. $Re = 80$ flow past main and control cylinders, $P/D = 2$, $T/D = 0.8$: pressure, streamfunction, and vorticity fields for the steady state solution.

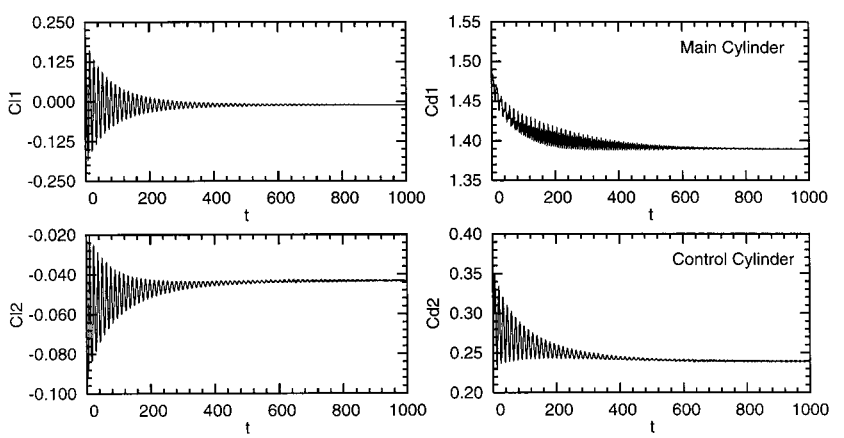

Figure 21. $Re = 80$ flow past main and control cylinders, $P/D = 2$, $T/D = 0.8$: time histories of the drag and lift coefficients for the main and control cylinders.

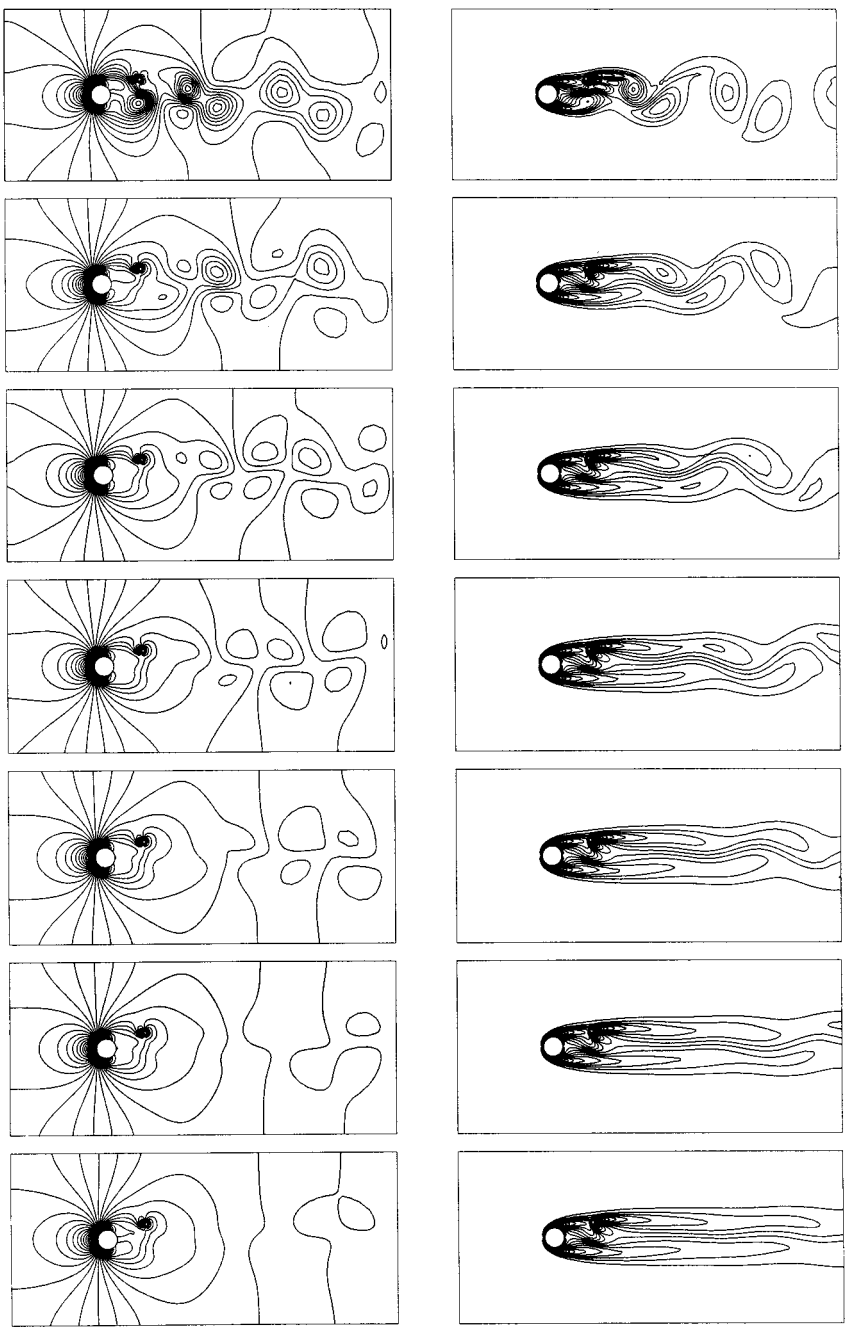

Figure 22. $Re = 80$ flow past main and control cylinders, $P/D = 2$, $T/D = 0.8$: pressure and vorticity fields at $t = 0$, 150, 300, 450, 600, 750, 900.

noticed that the stabilization of the flow begins close to the cylinders and then propagates downstream. This observation is in quite contrast to the start-up of flow past a single cylinder, where flow instability first develops downstream in the wake and then propagates upstream close to the cylinder. On comparing Figures 12 and 20 it can be observed that for the present case, the control cylinder causes the flow to deflect more towards the cylinder centerline. Similar observations were made by Strykowski and Sreenivasan [15].

To understand the effect of the placement of the control cylinder, the pressure coefficient (C_p) is plotted along the flow direction at a y location close to the shear layer of the main cylinder. This is done by projecting the finite element solution for the pressure field, computed on a mesh similar to the one shown in Figure 2, on a set of points taken at a section corresponding to $y/D = 0.65$ (y is measured with respect to the center of the cylinder). Figure 23 shows the variation of the pressure coefficient along the flow direction at $y/D = 0.65$ for various cylinder arrangements at $Re = 100$. From this figure it can be observed that the single cylinder case and the case involving the main and control cylinders with $P/D = 5$ and $T/D = 5$ give quite similar C_p distribution, as expected. One can observe a rise in pressure near the nose region of the cylinder, followed by a favorable pressure gradient as the flow accelerates over the windward side of the cylinder. The spatial variation in the pressure distribution in the wake caused by the vortex shedding can also be observed in the figure. For the control cylinder location corresponding to $P/D = 2$, $T/D = 1.0$ one can notice a change in the pressure distribution caused by the presence of control cylinder. This change is amplified for the case corresponding to $P/D = 2$, $T/D = 0.8$. For the $Re = 100$ case, the control cylinder seems to provide a local favorable pressure gradient in the wake, thereby stabilizing the shear layer locally. However, this effect is very local in nature and it can be observed that within about ten diameters downstream of the main cylinder the pressure distribution close to the shear layer assumes a similar form as that for a single cylinder. The drag–lift polars for all the cases for $Re = 100$ are shown in Figure 24. As has been observed before, the control cylinder causes a

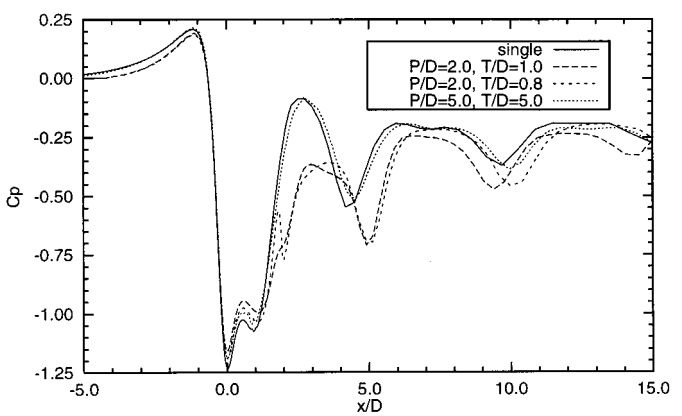

Figure 23. Streamwise variation of the pressure coefficient at $y/D = 0.65$ for $Re = 100$ flow for various arrangements of the main and control cylinders.

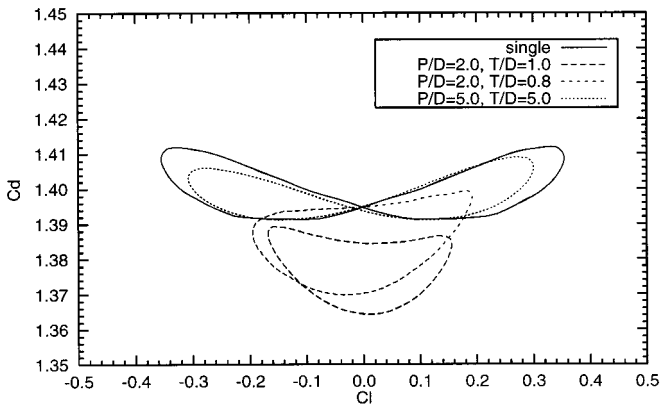

Figure 24. Drag–lift polars for the fully developed $Re = 100$ flow for various arrangements of the main and control cylinders.

marginal reduction in the amplitude of unsteady forces felt by the main cylinder. Additionally, in the presence of a control cylinder, the drag force acting on the main cylinder oscillates with the same frequency as the lift force. This effect of reduction in the frequency of the on-line force by a factor of two, may be of some significance in the context of civil structures where the failure due to fatigue loading is an important design criterion.

Shown in Figure 25 is the variation of the pressure coefficient along the flow direction at $y/D = 0.65$ for various cylinder arrangements at $Re = 80$. As has been seen for the $Re = 100$ case, in this case it can also be observed that the presence of a control cylinder leads to a local

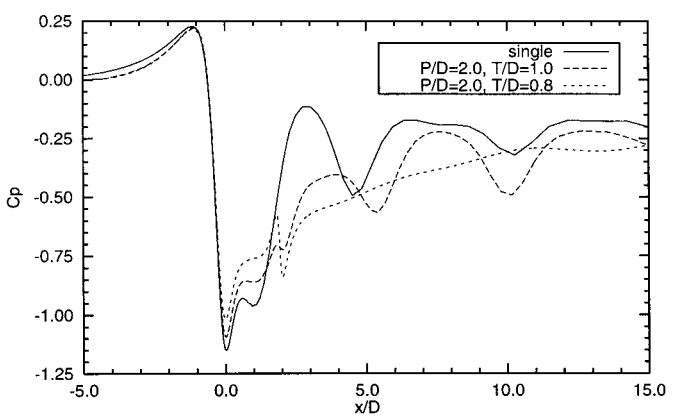

Figure 25. Streamwise variation of the pressure coefficient at $y/D = 0.65$ for $Re = 80$ flow for various arrangements of the main and control cylinders.

favorable pressure gradient that stabilizes the shear layer. The extent to which the shear layer is stabilized depends on the magnitude of the favorable pressure gradient created by the control cylinder. In the present case, the location of the control cylinder corresponding to $P/D = 2,\ T/D = 0.8$ leads to a complete suppression of the vortex shedding. However, from Figure 25 it can be observed that even for this case, the effect of the control cylinder on the pressure distribution reduces as one goes downstream of the cylinders. It is quite possible that if the computational domain in the present case is extended further downstream, the shear

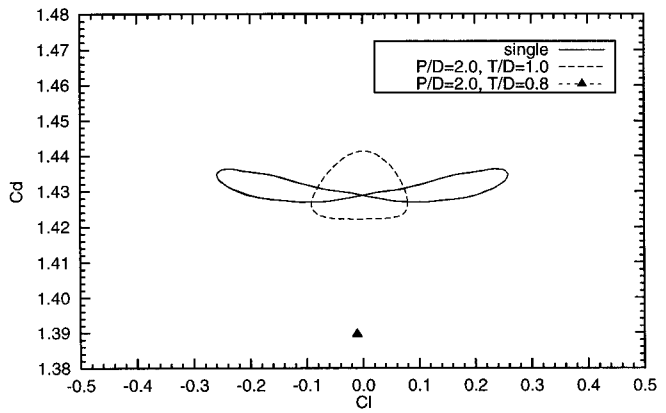

Figure 26. Drag–lift polars for the fully developed $Re = 80$ flow for various arrangements of the main and control cylinders.

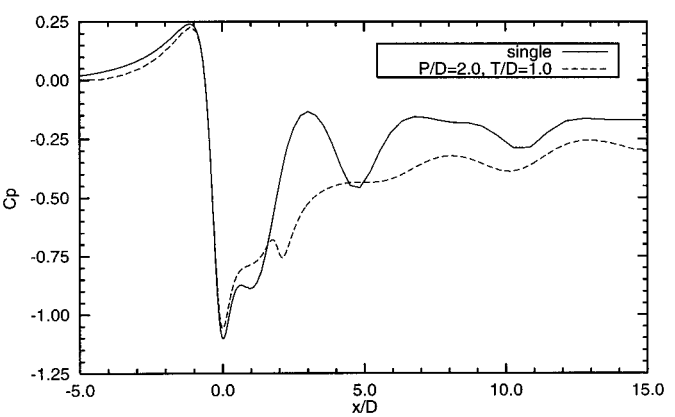

Figure 27. Streamwise variation of the pressure coefficient at $y/D = 0.65$ for $Re = 70$ flow for various arrangements of the main and control cylinders.

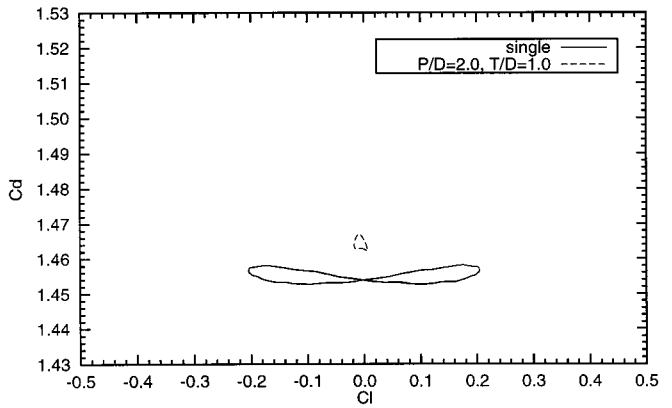

Figure 28. Drag–lift polars for the fully developed $Re = 70$ flow for various arrangements of the main and control cylinders.

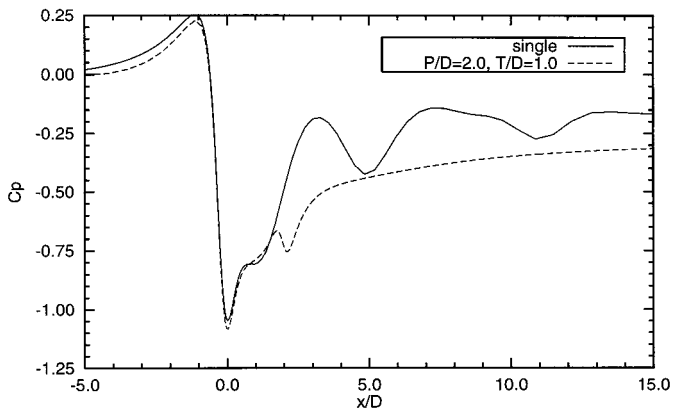

Figure 29. Streamwise variation of the pressure coefficient at $y/D = 0.65$ for $Re = 60$ flow for various arrangements of the main and control cylinders.

layer in the extended domain may become unstable and cause the flow to become unsteady. In fact, the flow visualization picture (Figure 3) in the article by Strykowski and Sreenivasan [15] shows a similar behavior. Figure 26 shows the drag–lift polars for all the cases that have been computed for $Re = 80$. The case corresponding to $P/D = 2$, $T/D = 0.8$, which leads to complete suppression of vortex shedding appears as a point on the drag–lift polar diagram. Figures 27 and 28 show respectively, the streamwise C_p distribution and drag–lift polars for $Re = 70$ flows while Figures 29 and 30 show results for $Re = 60$ flows.

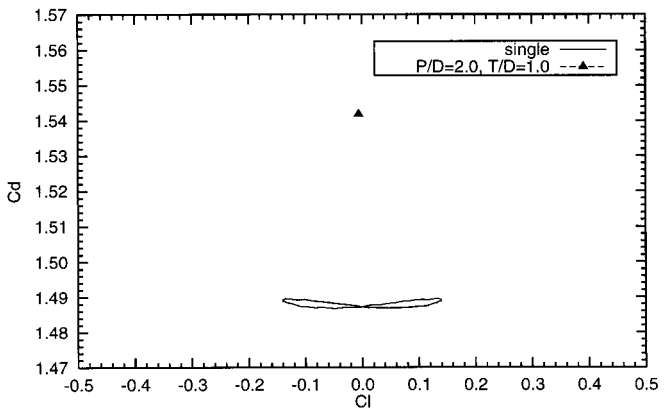

Figure 30. Drag–lift polars for the fully developed $Re = 60$ flow for various arrangements of the main and control cylinders.

5. CONCLUDING REMARKS

A numerical study has been carried out to study the effect of the placement of a control cylinder in the near wake of the main cylinder for flows at low Reynolds numbers. Results are compared with those from flow past a single cylinder at the corresponding Reynolds numbers. Excellent agreement is observed between the present computations and experimental findings of other researchers. It is seen that the proper placement of the control cylinder can lead to a complete suppression of the vortex-shedding behind the main cylinder. Even for the cases, where the complete suppression of unsteadiness does not take place, the control cylinder affects the flow past the main cylinder significantly. For example, the amplitude of the time varying forces is reduced and the drag coefficient oscillates at the same frequency as the lift coefficient for the main cylinder. The streamwise variation of the pressure coefficient is studies close to the shear layer of the main cylinder in order to investigate the cause of this phenomenon of flow control. It is observed that the control cylinder provides a local favorable pressure gradient in the wake region thereby stabilizing the shear layer locally. In certain cases, this favorable pressure gradient is quite weak and therefore, compared with the flow past a single cylinder, the destabilization of the shear layer is deferred to a small distance downstream. When the positioning of the control cylinder is such that the magnitude of the favorable pressure gradient is large, then the shear layer is rendered stable to a fairly large distance downstream of the cylinders. Locally, close to the cylinder, for such cases one sees a complete suppression of the vortex shedding. However, it is to be noted that this method of passive flow control is effective for small Reynolds number only. For practical applications, a control method that is effective at high Reynolds number needs to be studied. An effort to investigate the effect of rotating control cylinders, that inject momentum in the wake of the main cylinder, is underway. Our preliminary computations for Reynolds number $= 10^4$ indicate the technique to be very effective in reducing the drag on the cylinder. At high Reynolds

numbers, the three-dimensional effects in the flow become significant and it is suggested that three-dimensional simulations be carried out.

ACKNOWLEDGMENTS

Partial support for this work has come from the Department of Science and Technology, India under the project number DST-AE-95279 with Department of Aerospace Engineering, IIT Kanpur.

REFERENCES

1. Gad el Hak M, Bushnell DM. Separation control: review. *Journal of Fluids Engineering Transactions of the ASME* 1991; **113**: 5–29.
2. Griffin OM, Hall MS. Review—vortex shedding lock-on and flow control in bluff body wakes. *Journal of Fluids Engineering Transactions of the ASME* 1991; **113**: 526–537.
3. Zdravkovich MM. Review and classification of various aerodynamic and hydrodynamic means for suppressing vortex shedding. *Journal of Wind Engineering and Industrial Aerodynamics* 1981; **7**: 145–189.
4. Williamson CHK, Roshko A. Vortex formation in the wake of an oscillating cylinder. *Journal of Fluids and Structures* 1988; **2**: 355–381.
5. Ongoren A, Rockwell D. Flow structure from an oscillating cylinder. Part 1. Mechanisms of phase shift and recovery in the near wake. *Journal of fluid Mechanics* 1988; **194**: 197–223.
6. Ongoren A, Rockwell D. Flow structure from an oscillating cylinder. Part 2. Mode competition in the near wake. *Journal of Fluid Mechanics* 1988; **191**: 225–245.
7. Lecointe Y, Piquet J, Plantec J. Flow structure in the wake of an oscillating cylinder. In *Forum on Unsteady Flow Separation*, *FED-52*, Ghia KN (ed.). ASME: New York, 1987; 147–157.
8. Mittal S, Tezduyar TE. A finite element study of incompressible flows past oscillating cylinders and airfoils. *International Journal for Numerical Methods in Fluids* 1992; **15**: 1073–1118.
9. Tokumaru PT, Dimotakis PE. Rotary oscillation control of cylinder wake. *Journal of Fluid Mechanics* 1991; **224**: 77–90.
10. Tokumaru PT, Dimotakis PE. The lift of a cylinder executing rotary motions in a uniform flow. *Journal of Fluid Mechanics* 1993; **255**: 1–10.
11. Modi VJ, Mokhtarian F, Fernando MSUK. Moving surface boundary-layer control as applied to two-dimensional airfoils. *Journal of Aircraft* 1991; **28**: 104–112.
12. Modi VJ, Shih E, Ying B, Yokomizo T. Drag reduction of bluff bodies through momentum injection. *Journal of Aircraft* 1992; **29**: 429–436.
13. Munshi SR, Modi VJ, Yokomizo T. Aerodynamics and dynamics of rectangular prisms with momentum injection. *Journal of Fluids and Structures* 1997; **11**: 873–892.
14. Mittal S. Reduction of unsteady forces on bluff bodies using rotating control cylinders. In *IUTAM-Symposium on Mechanics of Passive and Active Flow Control*, Meier GEA, Viswanath PR (eds). Kluwer Academic Publishers: Dordrecht, 1999.
15. Strykowski PJ, Sreenivasan KR. On the formation and suppression of vortex 'shedding' at low Reynolds numbers. *Journal of Fluid Mechanics* 1990; **218**: 71–107.
16. Kim HB, Chang KS. Numerical study on vortex shedding from a circular cylinder influenced by a nearby control wire. *Computational Fluid Dynamics Journal* 1995; **4**(2): 151–164.
17. Morzynski M, Afanasiev K, Thiele F. Solution of the eigenvalue problems resulting from global non-parallel flow stability analysis. *Computer Methods in Applied Mechanics and Engineering* 1999; **169**: 161–176.
18. Zdravkovich MM. Review of flow interference between two circular cylinders in various arrangements. *Journal of Fluids Engineering Transactions of the ASME* 1977; **99**: 618–633.
19. Chen SS. *Flow-induced Vibrations of Circular Cylindrical Structures*. Hemisphere Publishing Corporation: New York, 1987.
20. Kim HJ, Durbin PA. Investigation of the flow between a pair of circular cylinders in the flopping regime. *Journal of Fluid Mechanics* 1988; **196**: 431–448.
21. Tokunaga H, Tanaka T, Satofuka N. Numerical simulation of viscous flows along multiple bodies by generalized vorticity–streamfunction formulation. *Computational Fluid Dynamics Journal* 1992; **1**: 58–66.
22. Williamson CHK. Evolution of a single wake behind a pair of bluff bodies. *Journal of Fluid Mechanics* 1985; **159**: 1.

23. Kiya M, Arie M, Tamura H, Mori H. Vortex shedding from two circular cylinders in staggered arrangement. *Journal of Fluids Engineering Transactions of the ASME* 1980; **102**: 166–173.
24. Kiya M, Mochizuki O, Ido Y, Suzuki T, Arai T. Flip-flopping flow around two bluff bodies in tandem arrangement. In *Bluff-body Wakes, Dynamics and Instabilities, IUTAM Symposium*, Göttingen, Germany, Eckelmann H, Graham JMR, Huerre P, Monkewitz PA (eds). Springer: Berlin, 1992; 15–18.
25. Mittal S, Kumar V, Raghuvanshi A. Unsteady incompressible flow past two cylinders in tandem and staggered arrangements. *International Journal for Numerical Methods in Fluids* 1997; **25**: 1315–1344.
26. Wu JC, Hu YC. Flow characteristics of tandem circular cylinders: effects of diameter ratio and longitudinal spacing. AIAA Paper 93-3088 (AIAA 24th Fluid Dynamics Conference, Orlando, FL), 1993.
27. Tezduyar TE, Mittal S, Ray SE, Shih R. Incompressible flow computations with stabilized bilinear and linear equal-order-interpolation velocity-pressure elements. *Computer Methods in Applied Mechanics and Engineering* 1992; **95**: 221–242.
28. Hughes TJR, Brooks AN. A multi-dimensional upwind scheme with no crosswind diffusion. In *Finite Element Methods for Convection Dominated Flows*, vol. 34, Hughes TJR (ed.). ASME: New York, 1979; 19–35.
29. Hughes TJR, Tezduyar TE. Finite element methods for first-order hyperbolic systems with particular emphasis on the compressible Euler equations. *Computer Methods in Applied Mechanics and Engineering* 1984; **45**: 217–284.
30. Mittal S. Stabilized space–time finite element formulations for unsteady incompressible flows involving fluid–body interactions. PhD thesis, University of Minnesota, 1992.
31. Saad Y, Schultz M. GMRES: a generalized minimal residual algorithm for solving nonsymmetric linear systems. *SIAM Journal of Scientific and Statistical Computing* 1986; **7**: 856–869.
32. Behr M, Liou J, Shih R, Tezduyar TE. Vorticity–streamfunction formulation of unsteady incompressible flow past a cylinder: sensitivity of the computed flow field to the location of the outflow boundary. *International Journal for Numerical Methods in Fluids* 1991; **12**: 323–342.
33. Behr M, Hastreiter D, Mittal S, Tezduyar TE. Incompressible flow past a circular cylinder: dependence of the computed flow field on the location of the lateral boundaries. *Computer Methods in Applied Mechanics and Engineering* 1995; **123**: 309–316.
34. Goldstein S. *Modern Developments in Fluid Dynamics*. Clarendon Press: Oxford, 1938.

